

## Galaxy Clustering in the CNOC2 Redshift Survey

R. G. Carlberg<sup>1,2</sup>, H. K. C. Yee<sup>1,2</sup>, S. L. Morris<sup>1,3</sup>, H. Lin<sup>1,2,4,5</sup>,  
P. Hall<sup>1,2</sup>, D. Patton<sup>1,6</sup>, M. Sawicki<sup>1,2,7</sup>, and C. W. Shepherd<sup>1,2</sup>

**Abstract.** The correlation evolution of a high luminosity subsample of the CNOC2 redshift survey is examined. The sample is restricted to galaxies for which the  $k$  corrected and evolution corrected  $R$  luminosity is  $M_R \leq -20$  mag, where  $M_* \simeq -20.3$  mag. This subsample contains about 2300 galaxies. In consort with 13000 galaxies in a similarly defined low redshift sample from the Las Campanas Redshift survey we find that the comoving correlation can be described as  $\xi(r|z) = (r_{00}/r)^\gamma (1+z)^{-(3+\epsilon)}$  with  $r_{00} = 5.08 \pm 0.08 h^{-1}$  Mpc,  $\epsilon = 0.02 \pm 0.23$  and  $\gamma = 1.81 \pm 0.03$  over the  $z = 0.03$  to  $0.65$  redshift range in a cosmology with  $\Omega_M = 0.2$ ,  $\Lambda = 0$ . The measured clustering amplitude, and its evolution, are dependent on the adopted cosmology. The evolution rates for  $\Omega_M = 1$  and flat low density models are  $\epsilon = 0.9 \pm 0.3$  and  $\epsilon = -0.5 \pm 0.2$ , respectively, with  $r_{00} \simeq 5h^{-1}$  Mpc in all cases.

### 1. Introduction

The measurement of the evolution of galaxy clustering is a direct test of theories for the formation of structure and galaxies in the universe. Within CDM-style structure formation theories galaxies form exclusively within dark matter halos whose clustering evolution should be slower than the underlying dark matter. Clustering evolution is of empirical and pragmatic interest on scales comparable to the size of galaxies themselves, since clustering leads to galaxy-galaxy merging of gas and stars which is a physical driver of galaxy evolution. On somewhat larger scales galaxy groups and clusters contain hot gas which exerts evolution pressures on galaxies.

---

<sup>1</sup>Visiting Astronomer, Canada–France–Hawaii Telescope, which is operated by the National Research Council of Canada, le Centre National de Recherche Scientifique, and the University of Hawaii.

<sup>2</sup>Department of Astronomy, University of Toronto, Toronto ON, M5S 3H8 Canada

<sup>3</sup>Dominion Astrophysical Observatory, Herzberg Institute of Astrophysics, , National Research Council of Canada, 5071 West Saanich Road, Victoria, BC, V8X 4M6, Canada

<sup>4</sup>Steward Observatory, University of Arizona, Tucson, AZ, 85721

<sup>5</sup>Hubble Fellow

<sup>6</sup>Department of Physics & Astronomy, University of Victoria, Victoria, BC, V8W 3P6, Canada

<sup>7</sup>Mail Code 320-47, Caltech, Pasadena 91125, USA

The theoretical groundwork to interpret the quantitative evolution of dark matter clustering and the qualitative trends of galaxy clustering evolution is largely in place for hierarchical structure models. Although the details of the mass buildup of galaxies and the evolution of their emitted light are far from certain at this time, clustering of galaxies depends primarily on the distribution of initial density fluctuations on the mass scale of galaxies. N-body simulations of ever growing precision and their theoretical analysis (Davis et al. 1985, Efsthathiou et al. 1985) have lead to a good semi-analytic understanding of dark matter clustering into the nonlinear regime. Normal galaxies, which are known to exist near the centers of dark matter halos with velocity dispersions in the approximate range of 50 to 250  $\text{km s}^{-1}$ , will not have a clustering evolution identical to the full dark matter density field (Kaiser 1984).

The observational measurement of clustering at higher redshifts is still maturing, with no published survey of the size, scale coverage, or redshift precision of the pioneering low redshift CfA survey (Davis & Peebles 1983). There are two redshift surveys extending out to  $z \simeq 1$ , the Canada France Redshift Survey (Lilly et al. 1995) and the Hawaii K survey (Cowie et al. 1996). Their redshift precision is insufficient for kinematic studies, however both quantify the substantial evolution in the luminosity function considerable population evolution. Measurement of the correlation evolution of the galaxies in these surveys found a fairly rapid decline in clustering with redshift (LeFèvre et al. 1996, Carlberg et al. 1997) although neither analysis took into account the evolution of the luminosity function or was able to quantify the effects of the small survey volumes.

## 2. The CNOC2 Sample

The Canadian Network for Observational Cosmology field galaxy redshift survey (CNOC2) is designed to investigate nonlinear clustering dynamics and its relation to galaxy evolution on scales smaller than approximately  $20h^{-1}$  Mpc over the  $0.1 \leq z \leq 0.7$  range. There is substantial galaxy evolution over this redshift range (Broadhurst, Ellis & Shanks 1988, Ellis et al. 1996, Lilly et al. 1995, Cowie et al. 1996, Lin et al. 1999). Investigating the clustering evolution of a population requires some basic ability to recover its progenitor hosts at higher redshift.

The observing and catalogue design procedures are adaptations and extensions of those for the CNOC cluster survey (Yee, Ellingson & Carlberg 1996, Yee et al. 1997). The CNOC2 survey is contained in four patches on the sky subtending a total sky area of about 1.55 square degrees. The sampled volume is about  $0.5 \times 10^6 h^{-3} \text{Mpc}^3$ , roughly comparable to the low redshift ‘‘CfA’’ survey used for similar measurements at low redshift (Davis & Peebles 1983) which had 1230 galaxies in the ‘‘semi-volume limited’’ Northern sample from which the correlation length was derived. The CNOC2 limiting magnitude of  $R = 21.5$  magnitude efficiently covers the redshift range targeted, 0.1 to about 0.7. The survey layout for the high luminosity subsample analyzed here is shown in Figure 1.

Photometry is obtained in the UBVRI bands, with the R band fixing the sample limit at 21.5 mag. The R filter stays redward of the 4000Å break over our redshift range. The other bands provide information useful for determining appropriate k-corrections and separating galaxies into types of different evolutionary state ( an issue not considered in this paper).

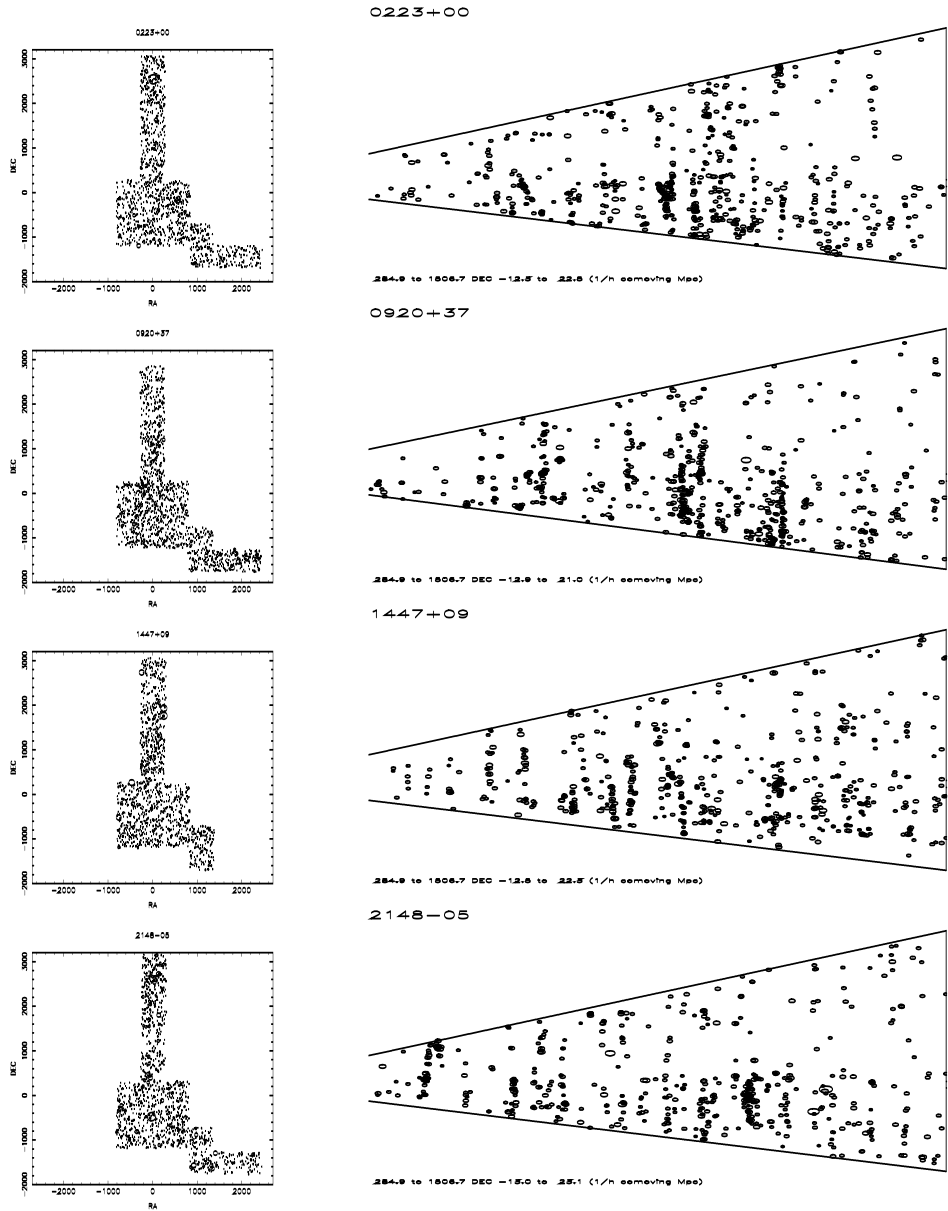


Figure 1. The layout of the high luminosity redshift sample,  $M_R^{ke} \leq -20$  mag, sample on the sky (left) and in co-moving distance (redshifts from 0.1 to 0.65) versus declination in comoving coordinates (right).

At low redshift we use the Las Campanas Redshift Survey (LCRS) to provide a directly comparable sample. The LCRS is an R band selected survey (Schechter et al. 1996) that covers the redshift range 0.033 to 0.15, with R band flux between 15.0 and 17.7 mag. The same correlation analysis programs were used with for the LCRS and CNOC2 data. The only differences are that the LCRS data are not k corrected and is only analyzed for a single cosmological model,  $q_0 = 0.1$ .

### 2.1. The High Luminosity Subsample

The evolution of correlations with redshift is sensitive to luminosity evolution. That is, usually the goal is to compare the evolution of the correlations of the same “primary” galaxies, which have likely evolved in luminosity as a result of stellar evolution of the existing stars, star formation, and merging of companion galaxies. Over the redshift range discussed here these effects are significant, but basically perturbative on a stable underlying population. In the absence of a luminosity correction one will be adding in galaxies of lower intrinsic mass with increasing redshift. Lower luminosity galaxies are less correlated (Carlberg et al. 1998, Loveday et al. 1995) which if over-represented in the higher redshift will lead to an erroneously rapid correlation evolution. From previous studies we concluded that the luminosity function can be approximated as evolving such that the absolute magnitude varies as  $M(z) = M(0) - Qz$  with  $Q \simeq 1$  (Lin et al. 1999). It should be noted that the this approach is a statistical correction designed to identify the same population at two redshifts and will work even for an evolving rate of bursting star formation, provided that evolution has no significant mass dependence. This assumption should be adequate for our high luminosity subsample (Lilly et al. 1995, Lin et al. 1999) but may fail for at lower luminosities. The volume density of galaxies makes no difference to the correlations. For the correlation analysis here we will use galaxies with  $M_R^{k,e} \leq -20$  mag, which defines a volume limited sample over the  $0.1 \leq z \leq 0.65$  range. The resulting sample (for  $q=0.1$ ) contains 2285 galaxies.

The LCRS data are evolution corrected with the same  $Q$  as the CNOC2 data, although at a mean redshift of about 0.1, this makes very little difference. The resulting low redshift sample contains 12467 galaxies that are used in the correlation analysis.

## 3. Real Space Correlations

The CNOC2 sample is designed to measure nonlinear clustering on scales of  $10h^{-1}$  Mpc and less. The clustering is quite naturally measured in terms of the two-point correlation function,  $\xi(r)$ , which measures the galaxy density excess above a random distribution,  $n_0$ . at distance  $r$  from a galaxy,  $n(r) = n_0[1 + \xi(r)]$  (Peebles 1980). Measurement of the real space function  $\xi(r)$  is not straightforward with redshift space data in any case, and yet more difficult with only a few hundred galaxies per redshift bin. The projected real space correlation function removes the peculiar velocities of redshift space at the cost of making a choice for the length of the redshift column over which the summation is done. Noting that the correlation function measures the fractional variance in galaxies in different

volumes we check as much as possible that our evaluation of the correlation does not artificially add or remove variance which will bias the result.

### 3.1. The Projected Real Space Correlation Function

The correlation function is a real space quantity, whereas the redshift space separation of two galaxies depends on their peculiar velocities as well as the physical separation. Although the peculiar velocities contain much useful information about clustering dynamics it is mainly a complication for the study of configuration space correlations. The peculiar velocities are eliminated by integrating over the redshift direction to give the projected correlation function,

$$w_p(r_p) = \int_{-R_p}^{R_p} \xi(\sqrt{r_p^2 + r_z^2}) dr_z \quad (1)$$

(Davis & Peebles 1983). If  $R_p = \infty$  and  $\xi(r)$  is a power law,  $\xi(r) = (r_0/r)^\gamma$ , then Equation 1 integrates to  $w_p(r_p)/r_p = \Gamma(1/2)\Gamma((\gamma - 1)/2)/\Gamma(\gamma/2)(r_0/r_p)^\gamma$  (Peebles 1980). However, in a practical survey summing over ever the entire redshift extent of the survey leads to little increase in the signal and growing noise from fluctuations in the field density. Here we are focussed on the non-linear correlations,  $\xi > 1$  which suggests we use  $R_p$  of several correlation lengths. A range of  $R_p$  and the resulting errors in  $r_{00}$  (see Equation 2 below) are displayed in Figure 2. We select  $R_p = 10h^{-1}$  Mpc as a conservative choice, having the largest (and most stable) errors. Similar results are obtained for any  $10h^{-1}$  Mpc  $\leq R_p \leq 50h^{-1}$  Mpc, but with increasing statistical fluctuations, most notably in the estimated errors of the fitted correlations.

The choice of a statistical estimator of the correlation function depends on the application. With point data the basic procedure is to determine the average number of neighboring galaxies within some projected radius and redshift distance  $R_p$ . We estimate  $w_p(r_p)$  using the simplest estimator,  $w_p = DD/DR - 1$  (Peebles 1980), which is accurate for the nonlinear clustering examined here and faster than methods which include the RR sum. The DD and DR sums extend over all four patches in CNOC2 and the six slices of LCRS, so that patch to patch variations in the mean volume density become part of the correlation signal. The patch to patch variation is used to estimate the error.

Estimated projected correlation functions, in co-moving co-ordinates using  $R_p = 10h^{-1}$  Mpc, are calculated for the LCRS galaxies bounded by redshifts [0.033, 0.15] and six redshift bins for the CNOC2 data, [0.10, 0.20, 0.26, 0.35, 0.40, 0.45, 0.55, 0.65]. The first CNOC2 redshift bin is the least populated with 185 galaxies and the fourth bin has the most with 602 galaxies. Relatively narrow redshift bins helps to reduce any problems associated with the detailed shape of the variation of  $n(z)$  over the redshift range of the bin. To fit the data to a specified function requires error estimates at each point.

The correlations are fit to the projection of the power law correlation function,  $\xi(r) = (r_0/r)^\gamma$  taking the errors to be the  $1/\sqrt{DD}$ , the weighted counts in each  $r_p$  bin. The fits use only the  $0.16 \leq r_p \leq 5.0h^{-1}$  Mpc range where there are minimal complications from slit crowding and small correlations. All results here are derived using co-moving co-ordinates, and normalized to a Hubble constant  $H_0 = 100h$  km s $^{-1}$  Mpc $^{-1}$ . The results displayed in Figure 3 are derived assuming a background cosmology of  $\Omega_M = 0.2, \Omega_\Lambda = 0$ .

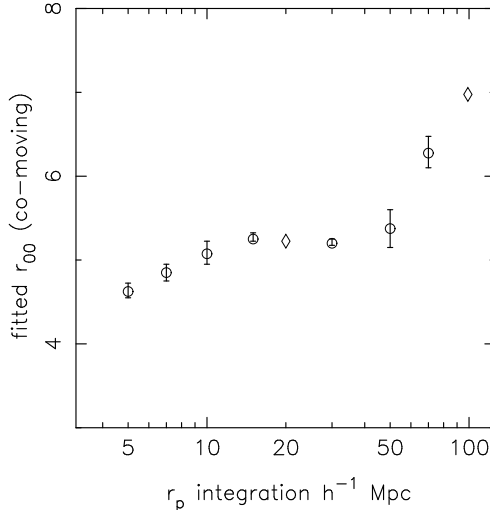


Figure 2. The derived  $r_{00}$  (see Eq. 2) as a function of the integration length,  $R_p$  used to define  $w_p(r_p)$ . The 90% confidence intervals are shown. The diamonds are plotted when  $\chi^2$  exceeds the formal level for 90% confidence. This most likely arises because the variances used to calculate  $\chi^2$  are estimated from the dispersion of the four patches, which will sometimes lead to erroneously small variances and hence large  $\chi^2$  values.

### 3.2. Errors of the Correlations

A straightforward approach to random error estimates is to take advantage of our sample being distributed over a number of separate patches. In each patch we fit four for CNOC2 and six for LCRS. The open circles are the results for the four individual patches CNOC2 fields (the individual LCRS slices are so similar that they are not displayed). The solid points give the result from the combined data, along with the estimated error.

As the size of a correlation survey grows there is a systematic increase in the derived correlation length. This is illustrated in Figure 3. The straight mean of the CNOC2  $r_0$  is  $3.2h^{-1}$  Mpc, the median is  $3.4h^{-1}$  Mpc, and the mean of  $r_0^7$  is  $3.5h^{-1}$  Mpc, whereas the four patches analyzed together find  $r_0$  is nearly  $4.0h^{-1}$  Mpc. This raises the question as to whether the correlations have converged within the current survey. We note that the expected variation from patch to patch for the given volumes with narrow redshift bins is about 45%, which is consistent the difference between a correlation length of 3.5 and  $4.3h^{-1}$  Mpc. In the combined sample with bigger bins we expect that there could be as much about 10% of the variance missing, which would boost the correlation lengths another 5%.

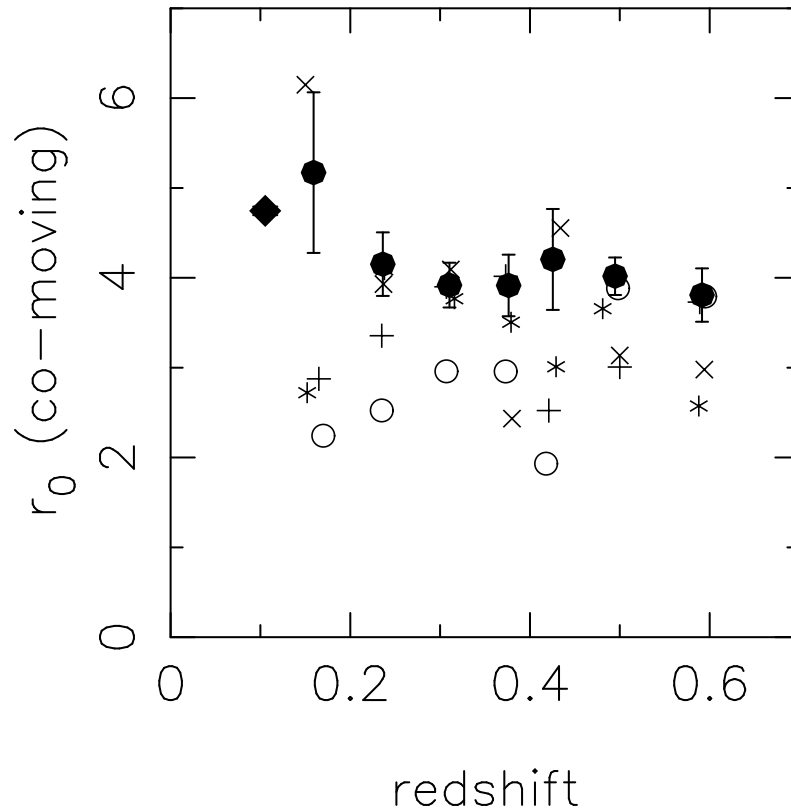


Figure 3. The correlation lengths (normalized to  $\gamma = 1.8$ ) as a function of redshift for  $\Omega_M = 0.2, \Omega_\Lambda = 0$ . The darkened diamond is from the LCRS with  $q=0.1$ . The errors are estimated from the variance of the four CNOC2 sky patches (shown with plus, asterisk, circle and cross symbols for the 0223, 0920, 1417 and 2148 patches, respectively) and the six LCRS slices (not shown since they are small). The solid points are the result of the combined correlation analysis of the four fields and are in general always larger than the mean of the individual fields, since they include the field to field variance.

#### 4. The Evolution of Galaxy Clustering

The evolution of correlations is conveniently described with the “epsilon” model,

$$r_0(z) = r_{00}(1+z)^{-(3+\epsilon-\gamma)/\gamma}, \quad (2)$$

where all lengths are in co-moving units. The parameter  $\epsilon$  measures the rate of growth of the mean physical density of neighboring galaxies. If  $\epsilon = 0$  then there is no change in the *physical* density with redshift. Positive  $\epsilon$  indicate a decline of clustered density with increasing redshift. The derived  $r_0(z)$  along with the estimated errors,  $\sigma(r_0(z))$  are fit to the  $\epsilon$  model with a formal  $\chi^2$  which reports both the suitability of the model and the parameter confidence interval.

The correlation lengths for the CNOC2 and LCRS analyzed in precisely the same way for our standard  $R_p = 10h^{-1}$  Mpc and  $Q = 1$  are shown in Figure 3. It is immediately clear that there is relatively little correlation evolution of this sample. It must be borne in mind that the sample is defined to be a similar set of galaxies with luminosities larger than about  $L_*$ , with luminosity evolution corrected, that accurately approximates a sample of fixed stellar mass with redshift. Samples which admit lower luminosity galaxies, or do not correct for evolution, or are selected in bluer pass bands where evolutionary effects are larger and less certainly corrected, will all tend to have lower correlation amplitudes.

The  $\epsilon$  model fits to the measured correlations are shown in Figure 4. The results are clearly a strong function of the cosmological world model. However, the strength of the correlations is truly impressive for any of the cosmologies. In the case of the low density flat model, the distances to the highest redshift galaxies are sufficiently large that the mean luminosity of the highest redshift galaxies is larger than those at lower redshifts. The best fit  $\epsilon$  values are  $0.02 \pm 0.23$  for  $\Omega_M = 0.2, \Omega_\Lambda = 0$ ,

At redshifts beyond 0.1 or so, the choice of cosmological model has a substantial effect on the correlation estimates. Relative to high matter density cosmological models, Low density and  $\Lambda$  models tend to have larger distances and volumes, which causes the correlations to be enhanced. The LCRS data are analyzed only within the  $q_0 = 0.1$  model. The correlations for three cosmologies, flat matter dominated, open, and low density  $\Lambda$ , are shown in Figure 3. The evolution rates for the flat and flat low density models are  $\epsilon = 0.9 \pm 0.3$  and  $\epsilon = -0.5 \pm 0.2$ , respectively, with  $r_{00} \simeq 5h^{-1}$  Mpc in all cases. These are marked with plus signs in Figure 4.

The effects of alternate values for the luminosity evolution are shown in Figure 4 with crosses indicating the results for  $Q = 0$  and  $Q = 2$ , with the adopted value being  $Q = 1$ . The absolute magnitude limit remains  $M_R = -20$  mag in all cases. In the absence of any allowance for luminosity evolution,  $Q = 0$ , galaxies of lower current epoch luminosity are increasingly included with redshift. Since lower luminosity galaxies are generally less correlated that leads to an artificially large  $\epsilon$ , the effect over this redshift range being very roughly  $\Delta\epsilon \approx 0.5\Delta Q$ .

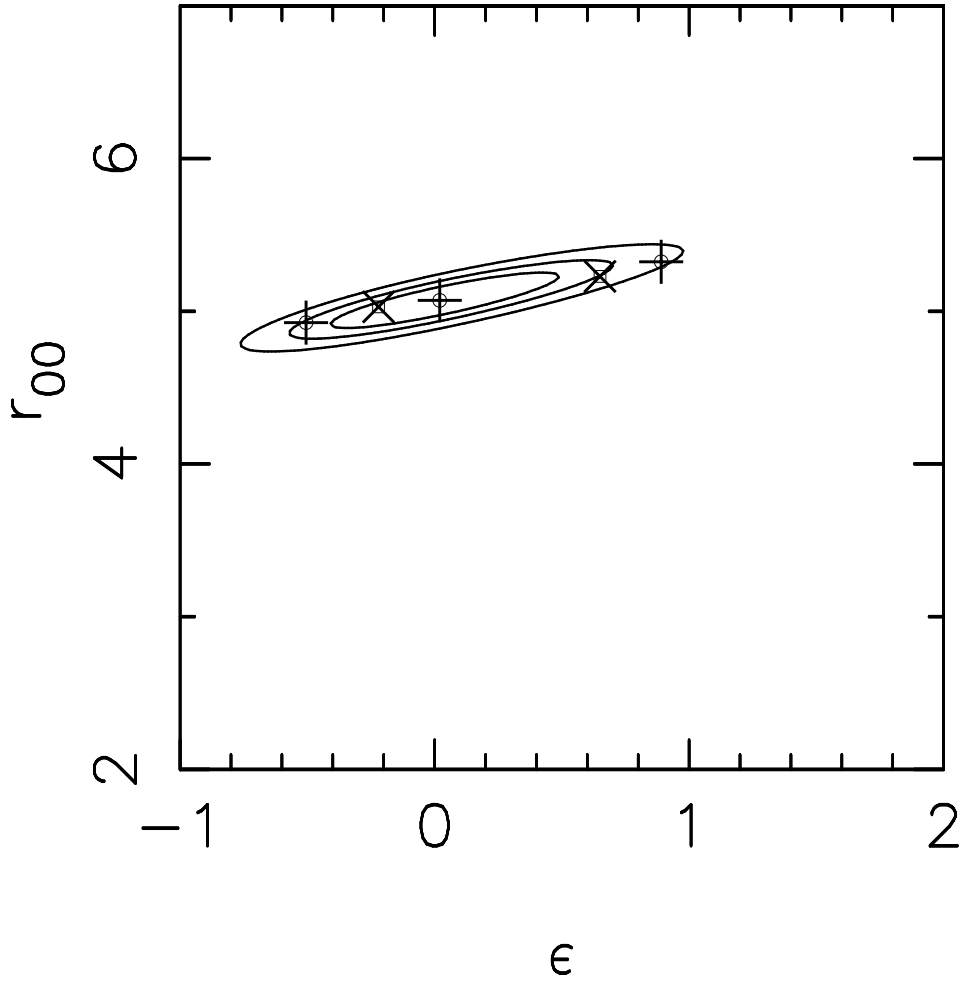


Figure 4. The  $\chi^2$  confidence levels for fits to the  $\epsilon$  model for the  $\Omega_M = 0.2, \Omega_\Lambda = 0$  model. The contours are for 68%, 90 and 99% confidence. The plus signs mark the results for  $\Omega_M = 1, \Omega_\Lambda = 0$ , peaking at  $\epsilon \simeq 0.6$  and  $\Omega_M = 0.2, \Omega_\Lambda = 0.8$  peaking at  $\epsilon = -0.4$ . The x's show the results for no evolution correction,  $Q = 0$ , in which case  $\epsilon = 0.65$ , and  $Q = 2$ , evolution, where  $\epsilon = -0.3$ .

## 5. Conclusions

The primary conclusion is that correlations evolve very weakly, if at all, with redshift. The main correlation results of this paper are contained in Figures 3. Out to redshift 0.65 the correlation evolution of high luminosity galaxies,  $k$  and evolution corrected, can be described with the double power law model,  $\xi(r|z) = (r_{00}/r)^\gamma(1+z)^{-(3+\epsilon)}$ , with  $r_{00} = 5.08 \pm 0.08h^{-1}$  Mpc,  $\epsilon = 0.02 \pm 0.23$  and  $\gamma = 1.81 \pm 0.03$ . There is no evidence in the current data for a change in the slope of the correlation function with redshift. The clustering results are consistent with galaxies being located in dark matter halos (Colin, Carlberg & Couchman 1997, Baugh et al. 1998, Colin et al. 1999) but are also consistent with “light-traces-mass” in low density universes where the mass clustering evolves very slowly with redshift.

Environmental factors clearly play a major role in the development of galaxies, as most clearly seen in the morphology-density relation (Dressler 1980, Hashimoto et al. 1998). We have established here that the neighborhood density, at separations between 0.1 and about  $5h^{-1}$  Mpc, is essentially non-evolving with increasing redshift. The implication is that any evolution in the population cannot be attributed to a significant change in the environmental density of neighboring galaxies. In a flat low-density model there is a slight rise of the mean density of neighbors into the past. The high luminosity luminous galaxies examined here do not as a population evolve much over the  $z \leq 1$  range (Lilly et al. 1995, Cowie et al. 1996, Lin et al. 1999) which could be the outcome of either no change in the environment, or, these galaxies being relatively insensitive to environmental change.

**Acknowledgments.** This research was supported by NSERC and NRC of Canada. We thank the CFHT Corporation for support, and particularly the telescope operators for their enthusiastic and efficient control of the telescope. HL acknowledges support provided by NASA through Hubble Fellowship grant #HF-01110.01-98A awarded by the Space Telescope Science Institute, which is operated by the Association of Universities for Research in Astronomy, Inc., for NASA under contract NAS 5-26555.

## References

- Baugh, C. M., Benson, A. J., Cole, S., Frenk, C. S., & Lacey, C. G. 1998, MNRAS, submitted (astro-ph/9811222)
- Broadhurst, T. J., Ellis, R. S., & Shanks, T. 1988, MNRAS, 235, 827
- Carlberg, R. G., Cowie, L. L., Songaila, A., & Hu, E. M. 1997, ApJ, 483, 538
- Carlberg, R. G., Yee, H. K. C., Morris, S. L., Lin, H., Sawicki, M., Wirth, G., Patton, D., Shepherd, C. W., Ellingson, E., Schade, D., Pritchet, C. J., & Hartwick, F. D. A. 1998, Phil. Trans. Roy. Soc. Lond. A. 357, 167
- Colin, P., Carlberg, R. G., & Couchman, H. M. P. 1997, ApJ, 390, 1
- Colin, P., Klypin, A., Kravtsov, A., & Khokhlov, A. 1999, ApJ, submitted (astro-ph/9809202)

- Cowie, L. L., Songaila, A., Hu, E. M., & Cohen, J. G. 1996, AJ, 112, 839
- Davis, M. & Peebles, P. J. E. 1983, ApJ, 267, 465
- Davis, M., Efstathiou, G., Frenk, C. S., & White, S. D. M. 1985, ApJ, 292, 371
- Dressler, A. 1980, ApJ, 236, 351
- Efstathiou, G., Davis, M., White, S. D. M., & Frenk, C. S. 1985, ApJS, 57, 241
- Ellis, R. S., Colless, M., Broadhurst, T., Heyl, J., & Glazebrook, K. 1996, MNRAS, 280, 235
- Hashimoto, Y., Oemler, A., J., Lin, H., & Tucker, D. L. 1998, ApJ, 499, 589
- Jenkins, A., et al. 1998, ApJ, 499, 20
- Kaiser, N. 1984, ApJ, 284, L9
- LeFèvre, O, Hudon, D., Lilly, S. J. Crampton, D., Hammer, F., & Tresse, L. 1996, ApJ, 461, 534
- Lilly, S. J., Tresse, L., Hammer, F., Crampton, D., & Le Fevre, O. 1995, ApJ, 455, 108
- Lin, H., Yee, H. K. C., Carlberg, R. G., Morris, S. L., Sawicki, M., Patton, D., Wirth, G., & Shepherd, C. W. 1998, ApJ, 518, 533
- Loveday, J., Maddox, S. J., Efstathiou, G., & Peterson, B. A. 1995, ApJ, 442, 457
- Jenkins, A., et al. 1999, ApJ, 521, L99
- Peebles, P. J. E. 1980, *Large Scale Structure of the Universe* (Princeton University Press: Princeton)
- Schechtman, S. A., Landy, S. D., Oemler, A., Tucker, D. L., Lin, H., Kirshner, R. P., & Schechter, P. L. 1996, ApJ, 470, 172
- Yee, H. K. C., Ellingson, E., & Carlberg, R. G. 1996, ApJS, 102, 269
- Yee, H. K. C., Sawicki, M., Carlberg, R. G., Lin, H., Morris, S. L., Patton, D. R., Wirth, G. D., Shepherd, C. W., Ellingson, E., Schade, D., & Marzke, R. in the proceedings for JD 11 “*Redshift Surveys in the 21st Century*” at the 23rd IAU General Assembly, Kyoto, 1997 (astro-ph/9710356)